Modelling Li^+ Ion Battery Electrode Properties

28 May 2009

Industrial Representatives: J. Ashmore & D. Clatterbuck (TIAX, LLC.)

Faculty: D.M. Anderson (George Mason), C.S. Bohun (Ontario), C. Breward (Oxford), J.D. Fehribach (WPI), L. Melara (Colorado, Boulder), C.P. Please (Southampton), G. Richardson (Nottingham), B. Vernescu (WPI)

Students: A. Arroyo (RPI), T. Bellsky (MSU), A.M. Bui Boi (SUNY Buffalo), H. Chi (SUNY Buffalo), I. Cipcigan (UMBC), M. Franklin (Claremont), L. Nguyen (Delaware), J. Siddique (George Mason), S. Swaminathan (Northwestern), O. Trichtchenko (McGill), Y. Wang (Delaware), C. Zhang (SUNY Buffalo)

Final Presentation given by M. Franklin, G. Richardson, C. Breward, J. Siddique & S. Swaminathan, 20 June 2008. Report prepared by G. Richardson, D.M. Anderson, S. Swaminathan & J.D. Fehribach.

1 Introduction

In recent years, interest in using lithium-ion (Li-ion) batteries as power sources for a wide range of devices (particularly portable devices) has grown significantly. There is thus a real need to understand at a fundamental level a wide range of battery performance criteria (energy density, power density, safety, durability, cost).

Our working group considered how to model the fundamental electrochemistry and transport of a simple Li-ion battery to obtain several basic mathematical results. We considered both a dilute-ion model for the electrolyte, as well as a model which assumes that Li ions are present in abundance (in excess). Both models assume Butler-Volmer interface reaction kinetics between the electrolyte and the solid electrodes (anode or cathode), and both are homogenized to obtain macroscale results. We also carried out a Monte Carlo simulation for transport in the solid electrode assuming that the electrolyte is a prefect conductor.

This report is divided into six sections: The next section presents a first-principles derivation of a mathematical model for ion transport and reaction kinetics in a simple porous-electrode battery (*cf.* Figure 1). Ion transport is by advection and diffusion, and the assumptions are appropriate for dilute ion concentrations. The standard charge-neutrality assumption is made in the electrolyte except in a narrow Debye layer near the solid electrode. The Debye layer is accounted for by a Butler-Volmer interface (boundary) condition. The model system is next non-dimensionalized, simplified and averaged to obtain integrals for the total current produced by the cell. Details of this averaging are presented in an appendix.

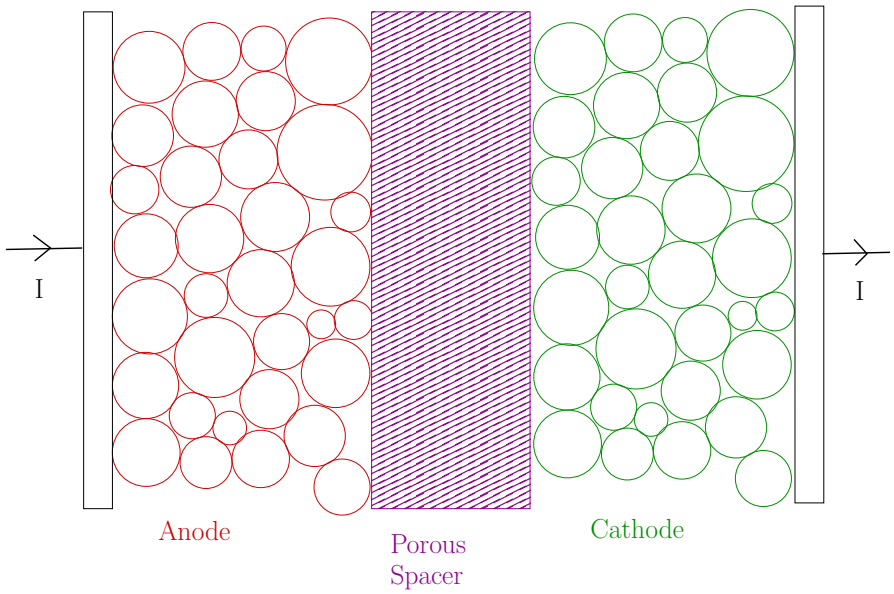

Figure 1: A schematic of the equilibrium configuration of the battery. The electrodes are formed of particles of the electrode material packed together. These are immersed in the electrolyte and contact between the two electrodes is avoided by placing a porous spacer between them through which only the electrolyte can percolate.

Section 3 then presents an electrochemical-potential model of the anode, cathode and electrolyte with the same fundamental assumptions as the first model, *except* that ions in the electrolyte are now assumed to be present in excess. This implies that transport in the electrolyte can be described by the Gauss law. The resulting system is then also non-dimensionalized, and the following section gives bounds for the homogenized effective conductivity for a steady-state version of this system. These bounds are derived through a variational formulation of a linearized version of the problem. Finally Section 5 presents an asymptotic analysis of a one-dimensional model for the battery, and Section 6 discusses the Monte Carlo simulation mentioned above.

2 Advection-diffusion modelling for ion concentration in a dilute electrolytic solution

The battery geometry. Typical lithium cells have two electrodes, composed of small particles of electrode material compressed together, which are bathed in an electrolyte containing lithium ions and separated by an insulating porous spacer, through which the electrolyte can permeate (see Figure 1).

2.1 Formulation

In this section we consider a model for a dilute binary electrolyte containing positive and negative ions species, with valence 1, and with concentrations c_p and c_n, respectively. At the electrodes, reactions take place in which one, or both, ion species are produced and/or consumed. Typically,

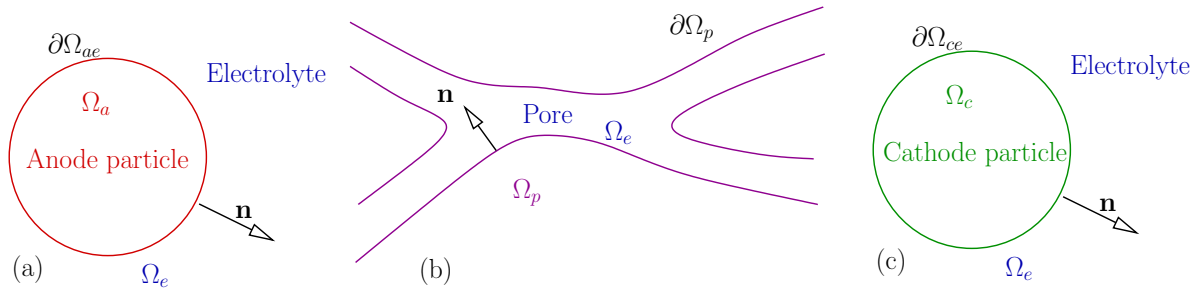

Figure 2: A schematic showing the domain of solution (a) surrounding an electrode particle and (b) in a pore.

such reactions produce or consume electrons leading to build up of charge on the electrode and, where both electrodes are connected through a resistive circuit, result in a current being driven through that circuit and the electrolyte (in which case the electrode and electrolyte in conjunction can be said to act as a battery). Alternatively a current may be forced through the electrolyte (by the application of an electromotive force across the electrodes) and the reactions at the electrodes driven in a particular direction (electrolysis).

The electrolyte bulk. In all but extremely narrow Debye layers (typical width 1nm) about the surface of the electrodes charge neutrality is almost exactly satisfied - that is $c_p \approx c_n$ (see, for example, [8] for further details). This motivates us to write $c_p \approx c$ and $c_n \approx c$ and write down the following (approximate) conservation equations, in the standard fashion, for the two ion species in the bulk of the electrolyte away from the Debye layers:

$$\left.\begin{aligned} d_*\tfrac{\partial c}{\partial t} + \nabla\cdot\boldsymbol{q}_p = 0, \quad d_*\boldsymbol{q}_p = -D_p\left(\nabla c + \tfrac{F}{R_gT}c\nabla\phi\right) \\ d_*\tfrac{\partial c}{\partial t} + \nabla\cdot\boldsymbol{q}_n = 0, \quad d_*\boldsymbol{q}_n = -D_n\left(\nabla c - \tfrac{F}{R_gT}c\nabla\phi\right) \end{aligned}\right\} \quad \text{in} \quad \Omega_e\,. \tag{1}$$

Here the left-hand equations represent the conservation of the two ion species with respective ion fluxes ($\boldsymbol{q}_p$ and $\boldsymbol{q}_n$) being given by the right hand equations. In the latter the the first term on the right-hand side represents a diffusive flux of ions while the second represents an advective flux occurring as a result of the action of the electric field $\boldsymbol{E} = -\nabla\phi$ upon the ions, where ϕ is the electric potential in the electrolyte. The parameters D_p, D_n, F, R_g and T are the diffusion coefficients of the positive and negative ions, Faraday's constant, the universal gas constant and absolute temperature, respectively. More details of the physical significance of these equations can be found, for example, in [8]. It is also useful to write down an equation for the current density $\boldsymbol{j}$ in terms of the ion fluxes

$$\boldsymbol{j} = F(\boldsymbol{q}_p - \boldsymbol{q}_n).$$

The electrodes. In the electrodes metallic lithium diffuses to (or from) its interface with the electrolyte where it is ionized and released into the electrolyte (or discharged and absorbed into the electrode) by the surface electrode reaction. We denote its concentration by c_s and write down

its conservation equation

$$\frac{\partial c_s}{\partial t} + \nabla \cdot \boldsymbol{q}_s = 0 \quad \text{and} \quad \boldsymbol{q}_s = -D_s \nabla c_s \qquad \text{in} \quad \Omega_a \quad \text{and} \quad \Omega_c, \tag{2}$$

noting that its motion is purely diffusive since lithium atoms are uncharged. In addition we must also evaluate the electric potential ψ in the electrode and here we make the simplest assumption (which is nevertheless pretty good), namely that the electrode is a sufficiently good conductor that we can neglect spatial variations in ψ and write

$$\psi = 0 \qquad \text{in} \quad \Omega_a \qquad \text{and} \qquad \psi = \Phi(t) \qquad \text{in} \quad \Omega_c. \tag{3}$$

Here, since electric potential is invariant under translation, we are allowed to set $\psi = 0$ on $x = 0$. The value of ψ on $x = L$ (*i.e.* $\psi = \Phi$) represents the total potential drop across the cell and is one of the key variables that will be determined from the solution to the model. This drop can be related to the current flowing in the circuit, via Ohm's Law, and hence to the current density, averaged over the electrode width, flowing into the electrode.

The electrode/electrolyte interfaces. Here we include the Debye layer, lying in the electrolyte immediately adjacent to the electrode, in the interface region. When adopting this approach it is standard to replace the complicated electrochemistry occurring in the Debye layer and on the electrode surface by a number of boundary conditions, including the so-called Butler-Volmer condition. In [8] a version of these conditions is systematically derived from an analysis of the underlying Poisson-Nernst-Planck (PNP) equations in the Debye layer. Here we merely state these conditions in terms of the reaction rate R upon the surface of the anode

$$\boldsymbol{n} \cdot \boldsymbol{q}_p = R, \quad \boldsymbol{n} \cdot \boldsymbol{q}_s = R, \quad \boldsymbol{n} \cdot \boldsymbol{q}_n = 0, \quad \text{on} \quad \partial\Omega_{ae}, \tag{4}$$

$$R = k_1 c_s \exp\left(-\frac{F}{2R_g T}(\phi - U(c_s))\right) - k_2 c \exp\left(\frac{F}{2R_g T}(\phi - U(c_s))\right)\Big|_{\partial\Omega_{ae}}. \tag{5}$$

Here the first condition relates the normal flux of lithium (positive) ions away from the electrode to the reaction rate R, the second states that the normal flux of lithium atoms into the electrode is equal to that of lithium ions away from it, the third states that the reaction produces no negative ions so that the normal flux of negative ions is zero and the fourth says that the Debye layer and electrode surface have zero net charge (ε_{el} and ε_s are the permittivities of the electrolyte and the electrode respectively). Also the anodic and cathodic transfer coefficients are taken to be $\alpha_a = \alpha_c = 1/2$. The final equation is the Butler-Volmer equation which is essentially phenomenological, but a version of which may be derived from analysis of the PNP equations in the Debye layer [8]. The constants k_p and k_n are reaction rate constants and the function $U(c_s)$, contained in the exponentials, is included to represent the effect of surface lithium ion concentration on the reaction rate (*cf.* Fuller *et al.* [3] for discussion and experimental results).

Similar equations hold on the cathode and can be written, where the reaction rate is denoted by S, in the form

$$\boldsymbol{n} \cdot \boldsymbol{q}_p = S, \quad \boldsymbol{n} \cdot \boldsymbol{q}_s = S, \quad \boldsymbol{n} \cdot \boldsymbol{q}_n = 0, \quad \text{on} \quad \partial\Omega_{ce}, \tag{6}$$

$$S = k_3 c_s \exp\left(-\frac{F}{2R_g T}(\phi - \Phi + V(c_s)\right) - k_4 c \exp\left(\frac{F}{2R_g T}(\phi - \Phi + V(c_s))\right)\Big|_{\partial\Omega_{ce}}. \tag{7}$$

Note that the functional form of $V(c_s)$ will, in general, be different to that of $U(c_s)$ because of the differences between the chemistry on the cathode and that on the anode.

The Butler-Volmer equations (5) and (7) can be simplified by writing it in terms of electrochemical potentials (*cf.* [7, pp. 16–19, 190–198], [1, 2]):

$$\iota = RF = \iota_0 \sinh\left(\frac{\mu_s - \mu_e}{2R_g T}\right)\Big|_{\partial\Omega_{ae}}, \tag{8}$$

$$\iota = SF = \iota_0 \sinh\left(\frac{\mu_s - \mu_e}{2R_g T}\right)\Big|_{\partial\Omega_{ce}}. \tag{9}$$

Here ι is the current density at the interface, ι_0 is the exchange current density (which is not necessary constant), and μ_s and μ_e are the electrochemical potentials for the solid electrode and electrolyte, respectively:

$$\mu_s := \mu_s^c, \tag{10}$$

$$\mu_e := \mu_e^c + F\phi, \tag{11}$$

where $\mu_\bullet^c$ are the chemical potentials in each phase. These chemical potentials depend on the ion concentrations (and temperature), but not the electrical potentials. The difference $\eta_s := \mu_s - \mu_e$ is termed the *surface overpotential* and constitutes the main "driving force" at the interface.

The edge of electrodes. At the left- and right- hand edges of the electrodes ($x = 0$ and $x = l$) the potential is constant and there is no flux of material either in or out of the electrolyte. We thus impose the boundary conditions

$$\boldsymbol{q}_p \cdot \mathbf{x}|_{x=0} = \boldsymbol{q}_n \cdot \mathbf{x}|_{x=0} = 0, \tag{12}$$

$$\boldsymbol{q}_p \cdot \mathbf{x}|_{x=l} = \boldsymbol{q}_n \cdot \mathbf{x}|_{x=l} = 0, \tag{13}$$

Here, since electric potential is invariant under translation, we are allowed to set $\psi = 0$ on $x = 0$. The value of ψ on $x = l$ (*i.e.* $\psi = \Phi$) represents the total potential drop across the cell and is one of the key variables that will be determined from the solution to the model. This drop can be related to the current flowing in the circuit, via Ohm's Law, and hence to the current density, averaged over the electrode width, flowing into the electrode.

The electrical circuit. The current I flowing in the circuit connected to this electrochemical cell is related to the reaction rates or current densities on the electrodes by

$$I = \int_{\partial\Omega_{ae}} \iota \, dA = F \int_{\partial\Omega_{ae}} R \, dA, \qquad \text{and} \qquad I = -\int_{\partial\Omega_{ce}} \iota \, dA = -F \int_{\partial\Omega_{ce}} S \, dA. \tag{14}$$

There are then two common scenarios. In the first of which I is specified, as in electrolysis and in the second I is related to the potential drop across the cell via, for example, Ohm's law

$$\Phi = \omega I, \tag{15}$$

where ω is the resistance of the circuit.

Electrochemical cells are typically constructed such that the distance between the conducting plate attached to the outer edges of the anode and that attached to the outer edge of the cathode

is small in comparison to the breadth of the cell. It is therefore frequently useful, from a practical point of view, to rewrite (14) in terms of the current flow, per unit area of the cell, $I/\mathcal{A}$ (here $\mathcal{A}$ is the cross-sectional area of the cell). Let $\partial\tilde{\Omega}_{ae}$ be the surface of electrode lying within a cylinder (pictured in Figure 3) with cross-sectional surface area L^2 and axis normal to the anode surface spanning the width of the anode; similarly let $\partial\tilde{\Omega}_{ce}$ be the surface of electrode lying within a cylinder with cross-sectional area L^2 and axis normal to the cathode surface spanning the width of the cathode. It follows that (14) now take the form

$$\frac{IL^2}{\mathcal{A}} = F\int_{\partial\tilde{\Omega}_{ae}} R dA, \qquad \text{and} \qquad \frac{IL^2}{\mathcal{A}} = -F\int_{\partial\tilde{\Omega}_{ce}} S dA. \tag{16}$$

Note that the dimensionless surface area of the electrode particles contained within $\tilde{\Omega}_{ae}$ and $\tilde{\Omega}_{ce}$ is of $O(\bar{B}L^3)$ where $\bar{B}$ is the typical electrode particle surface area per unit volume of electrode.

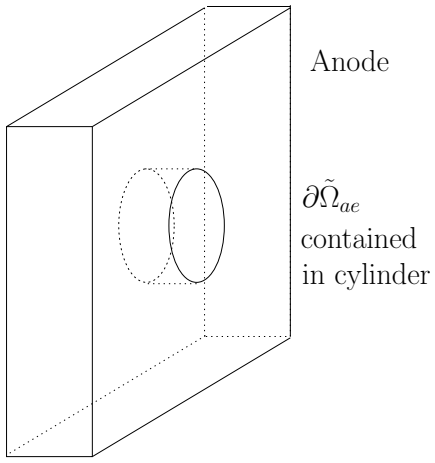

Figure 3: The cylinder containing $\partial\Omega_{ae}$.

The porous spacer. No reaction occurs on the edge of the porous spacer, which we assume is an inert insulating material. We thus consider the electrolyte equations (1)-(1) holding within the pores and impose the boundary conditions

$$\boldsymbol{n}\cdot\boldsymbol{q}_p = 0, \qquad \boldsymbol{n}\cdot\boldsymbol{q}_n = 0, \qquad \varepsilon_{el}\frac{\partial\phi}{\partial n} = \varepsilon_p\frac{\partial\psi}{\partial n} \qquad \text{on} \quad \partial\hat{\Omega}_p. \tag{17}$$

The potential within the the spacer material satisfies

$$\nabla^2\psi = 0. \tag{18}$$

2.2 Non-dimensionalization

Consider a cell with cross-sectional area $\mathcal{A}$ in which a current of typical magnitude $\bar{I}$; the typical current density is thus $\bar{J} = \bar{I}/\mathcal{A}$. Suppose further that the electrode widths are of $O(L)$ and that

they contain a volume fraction of electrode particles of $O(1)$ with typical particle surface area density (per unit volume) of $O(\bar{B})$. We now non-dimensionalize (1)-(13) and (15)-(16) as follows:

$$d_*c_s \sim \Pi_s, \quad d_*c \sim \Pi_0, \quad \boldsymbol{x} \sim L, \qquad t \sim \tau, \qquad d_*\psi \sim \bar{\Phi}, \qquad d_*\phi \sim \bar{\Phi}, \qquad I \sim \bar{J}\mathcal{A}, \qquad d_*\jmath \sim \bar{J},$$
$$\Phi \sim \bar{\Phi} \qquad U \sim \bar{\Phi}, \quad V \sim \bar{\Phi}, \quad d_*R \sim \tfrac{\bar{J}}{L\bar{B}F}, \quad d_*S \sim \tfrac{\bar{J}}{L\bar{B}F}, \quad d_*\boldsymbol{q}_s \sim \tfrac{\bar{I}}{L\bar{B}F}, \quad d_*\boldsymbol{q}_p \sim \tfrac{\bar{J}}{F}, \quad d_*\boldsymbol{q}_n \sim \tfrac{\bar{J}}{F}.$$

Here Π_s is the typical concentration of lithium atoms in the electrode, Π_0 is the typical concentration of lithium ions in the electrolyte, $\bar{\Phi}$ is the typical potential drop across the cell and $\bar{D}$ is a typical diffusivity in the electrolyte and τ is the typical timescale for discharge of the cell. Note that the ion fluxes have been non-dimensionalized with the current density divided by Faraday's constant $\bar{J}/F$ but that the flux of lithium atoms in the electrode and the reaction rates at the electrode surface are, however, estimated by dividing the current density by the typical total surface area of the electrode (*i.e.* $\bar{B}L$) multiplied by Faraday's constant. It remains to estimate the timescale τ for discharge of the cell. An estimate for the volume of the electrode is $L\mathcal{A}$ and it follows that the number of moles of lithium atoms is of $O(\Pi_s L\mathcal{A})$. The latter are consumed at a rate $\bar{J}\mathcal{A}/F$ and so the typical timescale for discharge of the cell is

$$\tau = \frac{F\Pi_s L}{\bar{J}}.$$

Proceeding with the non-dimensionalization leads to the following dimensionless model:

$$\left.\begin{aligned} &d_*\tfrac{\partial c}{\partial t} + \nu\nabla\cdot\boldsymbol{q}_p = 0, \quad d_*\boldsymbol{q}_p = -\gamma\kappa_p(\nabla c + \lambda c\nabla\phi) \\ &d_*\tfrac{\partial c}{\partial t} + \nu\nabla\cdot\boldsymbol{q}_n = 0, \quad d_*\boldsymbol{q}_n = -\gamma\kappa_n(\nabla c - \lambda c\nabla\phi) \end{aligned}\right\} \quad \text{in} \quad \Omega_e, \tag{19}$$

$$d_*\tfrac{\partial c_s}{\partial t} + \delta\nabla\cdot\boldsymbol{q}_s = 0, \quad d_*\boldsymbol{q}_s = -\tfrac{\gamma\nu}{\delta}\kappa_s\nabla c_s \quad \text{in} \quad \Omega_a \ , \tag{20}$$

$$\left.\begin{aligned} &d_*\boldsymbol{q}_p\cdot\boldsymbol{n} = \delta R, \qquad \boldsymbol{q}_n\cdot\boldsymbol{n} = 0, \qquad \boldsymbol{q}_s\cdot\boldsymbol{n} = R, \\ &d_*R = K_1c_s\exp\left(-\tfrac{\lambda}{2}(\phi - U(c_s))\right) - K_2c\exp\left(\tfrac{\lambda}{2}(\phi - U(c_s))\right) \end{aligned}\right\} \quad \text{on} \quad \partial\Omega_{ae} \tag{21}$$

$$d_*\tfrac{\partial c_s}{\partial t} + \delta\nabla\cdot\boldsymbol{q}_s = 0, \quad d_*\boldsymbol{q}_s = -\tfrac{\gamma\nu}{\delta}\kappa_s\nabla c_s \quad \text{in} \quad \Omega_c \ , \tag{22}$$

$$\left.\begin{aligned} &d_*\boldsymbol{q}_p\cdot\boldsymbol{n} = \delta S, \qquad \boldsymbol{q}_n\cdot\boldsymbol{n} = 0, \qquad \boldsymbol{q}_s\cdot\boldsymbol{n} = S, \\ &d_*S = K_3c_s\exp\left(-\tfrac{\lambda}{2}(\phi - \Phi + V(c_s))\right) - K_4c\exp\left(\tfrac{\lambda}{2}(\phi - \Phi + V(c_s))\right) \end{aligned}\right\} \quad \text{on} \quad \partial\Omega_{ce} \tag{23}$$

$$\begin{aligned} &\boldsymbol{q}_p\cdot\mathbf{x} = 0, \quad \boldsymbol{q}_n\cdot\mathbf{x} = 0, \quad \text{on} \quad x = 0 \\ &\boldsymbol{q}_p\cdot\mathbf{x} = 0, \quad \boldsymbol{q}_n\cdot\mathbf{x} = 0, \quad \text{on} \quad x = \Lambda, \end{aligned} \tag{24}$$

$$I = \delta\int_{\partial\tilde{\Omega}_{ae}} R dA, \qquad I = -\delta\int_{\partial\tilde{\Omega}_{ce}} S dA, \tag{25}$$

$$\text{Either} \quad I \quad \text{specified}, \quad \text{or} \quad \Phi = I, \tag{26}$$

(note that where we use Ohm's law to determine the current we choose $\bar{I} = \bar{\Phi}/\omega$). Here the

dimensionless parameters are given by

$$\begin{gathered} d_*\lambda = \tfrac{F\bar{\Phi}}{R_gT}, \qquad d_*\kappa_p = \tfrac{D_p}{\bar{D}}, \qquad d_*\kappa_n = \tfrac{D_n}{\bar{D}}, \qquad d_*\kappa_s = \tfrac{D_s}{\bar{D}}, \\ d_*\delta = \tfrac{1}{\bar{B}L}, \qquad d_*\gamma = \tfrac{F\Pi_0\bar{D}}{\bar{J}L}, \qquad d_*\nu = \tfrac{\Pi_s}{\Pi_0}, \qquad d_*\Lambda = \tfrac{l}{L} \\ d_*K_1 = \tfrac{k_1\Pi_s\bar{B}LF}{\bar{J}}, \quad d_*K_2 = \tfrac{k_2\Pi_0\bar{B}LF}{\bar{J}}, \quad d_*K_3 = \tfrac{k_3\Pi_s\bar{B}LF}{\bar{J}}, \quad d_*K_4 = \tfrac{k_4\Pi_0\bar{B}LF}{\bar{J}}. \end{gathered} \tag{27}$$

Here δ is a geometric parameter giving a measure of the electrode particle surface area per unit area of the cell; λ gives the ratio of a typical potential drop across the cell to the thermal voltage; κ_p, κ_n and κ_s are the dimensionless diffusivities of positive (Li^+) ions, negative ions and lithium atoms, respectively; γ gives a measure of the ratio of the maximum sustainable flux of ions in the electrolyte to the actual ion flux; δ measures the ratio of the total electrode particle surface area to the surface area of the cell; ν is the ratio of typical lithium concentrations in the solid to those in the electrolyte; and K_1, K_2, K_3 and K_4 are dimensionless reaction rates. The parameter δ appears in (25) and ensures that the right-hand sides of these equations is of $O(1)$; the surfaces $\partial\tilde{\Omega}_{ae}$ and $\partial\tilde{\Omega}_{ce}$ have dimensionless area $O(1/\delta)$.

Remarks. Here we have non-dimensionalized so that the dimensionless fluxes $\boldsymbol{q}_n$, $\boldsymbol{q}_p$ and $\boldsymbol{q}_s$ are typically all $O(1)$. In addition, we note that the dimensionless parameter λ (representing the ratio of the typical voltage drop across the cell to the thermal voltage) will play a particularly important role in the analysis that follows. The thermal voltage R_gT/F is, at room temperature about 25mV and so λ will be large in most applications. Furthermore we remark that the factors δ appearing in equations (25) ensure that the right-hand sides of these equations are of $O(1)$, the dimensionless surface areas of $\partial\Omega_{ae}$ and $\partial\Omega_{ce}$ being of $O(1/\delta)$.

2.2.1 Size of dimensionless parameters

We start by putting down some rough estimates for the sizes of the important dimensional parameters in the problem

$$\begin{gathered} d_*\tfrac{R_gT}{F} \approx 0.025\text{V}, \qquad d_*D_p \approx 10^{-11} \quad \text{or perhaps} \quad 10^{-9}\text{m}^2\ \text{s}^{-1}, \quad d_*D_n \approx \tfrac{D_p}{3}\text{m}^2\ \text{s}^{-1}, \quad d_*D_s \approx 10^{-12}\text{m}^2\ \text{s}^{-1}, \\ \Pi_0 \approx 10^3\text{mol m}^{-3}, \quad \Pi_s \approx 50\times 10^3\text{mol m}^{-3}, \qquad a \approx 10^{-5}\text{m}, \qquad L \approx 1.5\times 10^{-4}\text{m}, \end{gathered}$$

where a gives a typical radius of an electrode particle and the figures for D_p (in aqueous solution) and D_s come from [11] and [4], respectively. We now use these dimensional parameters to estimate the key dimensionless parameters

$$\lambda \approx 180, \quad \kappa_p = 1, \quad \kappa_n \approx 1/3, \quad \kappa_s \approx 10^{-1}, \quad \nu \approx 50.$$

We have little information about the sizes of the dimensionless reaction constants K_1, K_2, K_3 and K_4. However as long as their sizes are not excessively large or small this makes little difference since the exponentials in (21)-(23) are contain the large parameter λ and thus are expected to be dominant.

The geometric parameter δ. The parameter δ, gives the surface area density of electrode particles per unit surface area of the cell and depends crucially on particle size. We can estimate δ for a collection of uniform spheres of radius a; in particular we consider body centred cubic packing (the spheres are centred at the corners of a cubic lattice) and close packing arrangements, such as face-centred cubic packing and hexagonal close packing, in which the spheres are packed as densely as possible:

$$\text{body centred cubic} \qquad \delta = \frac{\sqrt{2}a}{\pi L}, \qquad \text{close packing} \qquad \delta = \frac{2a}{\pi L}. \tag{28}$$

Referring to the rough estimates provided above a/L is typically about $1/15$ and δ roughly $1/20$–$1/50$.

2.3 Simplifications of the equations and boundary conditions

Equations (19) can be rearranged to give an equation solely in terms of c and similarly ϕ can be eliminated from the boundary conditions (21a)-(21b) and (23a)-(23b) to give

$$\frac{\partial c}{\partial t} = 2\gamma\nu \frac{\kappa_n \kappa_p}{\kappa_n + \kappa_p} \nabla^2 c \qquad \text{in} \quad \Omega_e, \tag{29}$$

$$\left.\frac{\partial c}{\partial n}\right|_{\partial\Omega_{ae}} = -\frac{\delta R}{2\gamma\kappa_p}, \qquad \left.\frac{\partial c}{\partial n}\right|_{\partial\Omega_{ce}} = -\frac{\delta S}{2\gamma\kappa_p}. \tag{30}$$

And thus if we know the reaction rates R and S this provides a closed system for c in Ω_e. Similarly we can find equations and boundary conditions for ϕ; these are

$$\nabla \cdot (c\nabla\phi) = \frac{1}{\lambda}\frac{\kappa_n - \kappa_p}{\kappa_n + \kappa_p}\nabla^2 c, \tag{31}$$

$$c\left.\frac{\partial \phi}{\partial n}\right|_{\partial\Omega_{ae}} = -\frac{\delta R}{2\lambda\gamma\kappa_p}, \qquad c\left.\frac{\partial \phi}{\partial n}\right|_{\partial\Omega_{ce}} = -\frac{\delta S}{2\lambda\gamma\kappa_p}, \tag{32}$$

2.4 Averaging in the electrolyte

Multiple-scales formalism. There are two disparate lengthscales in this problem corresponding to that of the electrode particles ($O(\delta)$ in dimensionless units) and that of the electrolytic cell ($O(1)$ in dimensionless units). In order to analyze the problem it is helpful to introduce a microscale variable $\hat{\boldsymbol{x}}$ on the particle lengthscale. Furthermore we assume that there is *local* periodicity in the electrode particle arrangement and, in particular, that the structure is periodic within a repeating domain $\hat{V}_{per} \cup \hat{\Omega}_{per}$ (see Figure 6). In fact, in order to keep the treatment as general as possible, we shall allow the shape and size of the particles (denoted by $\hat{\Omega}_{per}$) to vary over the long lengthscale $\boldsymbol{x}$ but, as a consequence of the multiple scale method we employ, we require that the union of the domain occupied by the particles $\hat{\Omega}_{per}$ and that occupied by the electrolyte lying outside them $\hat{V}_{per}$ to be strictly periodic. Rather than rescale $\boldsymbol{x}$ with δ directly we rescale with δp where δp measures the size of the periodic domain $\hat{V}_{per} \cup \hat{\Omega}_{per}$ (*e.g.* the length of its edges where it is cuboidal) and p is an $O(1)$ parameter. Thus the microscale variable is defined by

$$\boldsymbol{x} = \delta p \hat{\boldsymbol{x}}, \tag{33}$$

and the gradient operator transforms according to $\nabla \to \nabla + \hat{\nabla}/(\delta p)$. These definitions are used in the appendix to derive homogenized versions of the equations for ion concentration c and electric potential ϕ within the electrolyte by using the method of multiple scales.

The homogenized equations. We apply the method of multiple scales in appendix A to write down an averaged equation for the diffusion of lithium ions in the electrolyte and the potential in the electrolyte. By comparing (29)-(32) to (70)-(72) we can identify

$$D = 2\gamma\nu\frac{\kappa_n\kappa_p}{\kappa_n+\kappa_p}, \qquad \epsilon = \delta p \qquad k = \frac{\nu\kappa_n}{p(\kappa_n+\kappa_p)}, \qquad \alpha = \frac{\kappa_n-\kappa_p}{\kappa_n+\kappa_p}.$$

By analogy with (85) and (90), the averaged equation for c and ϕ in the electrodes are

$$\mathcal{V}\frac{\partial c}{\partial t} = 2\gamma\nu\frac{\kappa_n\kappa_p}{\kappa_n+\kappa_p}\frac{\partial}{\partial x_i}\left(\mathcal{B}_{ij}\frac{\partial c}{\partial x_j}\right) + \frac{\nu\kappa_n}{p(\kappa_n+\kappa_p)}\tilde{Q}, \tag{34}$$

$$\frac{\partial}{\partial x_i}\left(\mathcal{B}_{ij}\left(\lambda c\frac{\partial\phi}{\partial x_j} - \left(\frac{\kappa_n-\kappa_p}{\kappa_n+\kappa_p}\right)\frac{\partial c}{\partial x_j}\right)\right) + \frac{\tilde{Q}}{p\gamma(\kappa_n+\kappa_p)} = 0. \tag{35}$$

where $\mathcal{B}_{ij}$ is defined in (86) and

$$\tilde{Q} = \begin{cases} d_* \int_{\partial\hat{\Omega}_{per}} R d\hat{S} & \text{in the anode} \\ d_* \int_{\partial\hat{\Omega}_{per}} S d\hat{S} & \text{in the cathode} \end{cases}$$

2.5 Rescaling of the solid diffusion equations about a single electrode particle

Rescaling distances in (21) and (23) by δp (which is of the order of the particle dimensions) via (33) we obtain

$$\frac{\partial c_s}{\partial t} = \Gamma\hat{\nabla}^2 c_s, \qquad \boldsymbol{q}_s = -\Gamma\hat{\nabla}c_s, \qquad \left.\frac{\partial c_s}{\partial\hat{n}}\right|_{\partial\hat{\Omega}_{per}} = -\frac{Q}{\Gamma}, \tag{36}$$

where $Q = R$ in the anode and $Q = S$ in the cathode. Note that since we consider diffusion of lithium within a single particle (there is no diffusion between particles), $\nabla \to \hat{\nabla}/(\delta p)$. The parameter $\Gamma = \gamma\nu\kappa_s/p^2\delta^2$ is important and can be expressed, on referring back to (28), in the form

$$\Gamma = \frac{\gamma\nu\kappa_s}{p^2\delta^2} = \frac{F\Pi_s D_s\bar{A}}{\mathcal{J}a} \times (O(1) \ \text{ constant}),$$

where $\mathcal{J}$ is the typical current density on the surface of the particle. It can thus be seen to play the role of γ inside the electrode giving the ratio of the maximum sustainable flux of Lithium atoms to the actual atomic flux.

2.6 The current equations

Consider now the equations relating the current to the reaction rates (25). The volume of each microscale periodic domain $\hat{V}_{per} \cup \hat{\Omega}_{per}$ on the microscale is $(\delta p)^3(\int_{\hat{V}_{per}} d\hat{V} + \int_{\hat{\Omega}_{per}} d\hat{V})$ which we rewrite in the form $(\delta p)^3(\mathcal{V} + |\hat{\Omega}_{per}|)$. The number of microscale periodic domains contained within a macroscopic volume dV is thus $dV/((\delta p)^3(\mathcal{V} + |\hat{\Omega}_{per}|))$. On recalling that $\partial\Omega_{ae}$ is the electrode surface contained in a cylinder of unit cross-sectional area between $x = 0$ and $x = 1$ while $\partial\Omega_{ce}$ is

the electrode surface contained in a cylinder of unit cross-sectional area between $x = 1$ and $x = \Lambda$ it follows that

$$\int_{\partial\tilde{\Omega}_{ae}} RdA = \int_0^1 (\delta p)^2 \left(\int_{\partial\hat{\Omega}_{per}} Qd\hat{S} \right) \frac{dx}{(\delta p)^3(\mathcal{V} + |\hat{\Omega}_{per}|)},$$
$$\int_{\partial\tilde{\Omega}_{ce}} RdA = \int_1^\Lambda (\delta p)^2 \left(\int_{\partial\hat{\Omega}_{per}} Sd\hat{S} \right) \frac{dx}{(\delta p)^3(\mathcal{V} + |\hat{\Omega}_{per}|)}.$$

In turn this can be rewritten as

$$\int_{\partial\tilde{\Omega}_{ae}} RdA = \frac{1}{\delta p} \int_0^1 \frac{\tilde{R}}{\mathcal{V} + |\hat{\Omega}_{per}|} dx \qquad \int_{\partial\tilde{\Omega}_{ce}} SdA = \frac{1}{\delta p} \int_1^\Lambda \frac{\tilde{S}}{\mathcal{V} + |\hat{\Omega}_{per}|} dx.$$

Hence we can rewrite (25) in terms of the locally averaged reaction rates $\tilde{R}$ and $\tilde{S}$ as

$$I = \frac{1}{p} \int_0^1 \frac{\tilde{R}}{\mathcal{V} + |\hat{\Omega}_{per}|} dx, \qquad I = \frac{1}{p} \int_1^\Lambda \frac{\tilde{S}}{\mathcal{V} + |\hat{\Omega}_{per}|} dx.$$

3 Excess-ion electrolytic modelling

Assumptions. Most of the assumptions discussed in the previous section (geometry, Butler-Volmer kinetics, perfect solid conduction) continue to be made here. The only exception is that now the Li ions are assumed to be present in the electrolyte in excess. This is the opposite of assuming dilute ion concentrations, and it may be less appropriate for polymer electrolytes, but it leads to a particularly simple model.

3.1 Electrolyte transport

Given that the ions (positive and negative) are present in excess in the electrolyte, their concentrations and chemical potentials are essentially constant. Thus the electrochemical potential gradient in the electrolyte is proportional to the electrical potential gradient,

$$\nabla\mu_e = F\nabla\phi \tag{37}$$

and transport in the electrolyte is by electrical conduction only. Thus the equation for μ_e is given by the Gauss law:

$$0 = \nabla(\sigma\nabla\mu_e) \tag{38}$$

where σ is the electrical conductivity of the electrolyte.

3.2 Potential system

Let $u := \mu_e/2R_gT$ and $v := \mu_s/2R_gT$ be the non-dimensional electrochemical potentials in the electrolyte and solid respectively. One can then derive a potential model for the battery:

$$0 = \nabla(\sigma\nabla u), \quad \text{in} \quad \Omega_e, \tag{39}$$

$$\frac{\partial v}{\partial t} = \nabla(\kappa_s\nabla v), \quad \text{in} \quad \Omega_a,\ \Omega_c, \tag{40}$$

$$-\sigma\nabla\mu_e \cdot \boldsymbol{n} = -\kappa_s\nabla\mu_s \cdot \boldsymbol{n} = \iota F = \iota_0 F \sinh(v - u), \quad \text{on} \quad \partial\Omega_{ae},\ \partial\Omega_{ce}, \tag{41}$$

The electrochemical conductivity κ_s in the solid electrode is proportional to the diffusivity D_s:

$$\kappa_s = \frac{2F^2 D_s}{\partial \mu_s / \partial c_s} \tag{42}$$

where the partial derivative is given by a constitutive relation. If the Li atoms obey the ideal gas law, then

$$\mu_s = \mu_s^c = \mu_s^{eq} + R_g T \ln\left(\frac{c_s}{c_s^{eq}}\right) . \tag{43}$$

This system (39–41) must be coupled with far-field conditions equivalent to (24–26) to give a complete potential model for the battery, but these far-field conditions will not be a part of the discussion in this section or the next, so they are not specifically defined here.

The potential system (39–41) can be non-dimensionalized using the same length and time scales as before, and the following dimensionless parameters: $\epsilon := \kappa_s/\sigma$ and $i_0 = \iota_0 FL/2R_g T\sigma$. Using these parameters, one obtains a non-dimensional potential system:

$$0 = \nabla^2 u, \quad \text{in} \quad \Omega_e, \tag{44}$$

$$\frac{\partial v}{\partial t} = \nabla(\epsilon \nabla v), \quad \text{in} \quad \Omega_a,\ \Omega_c, \tag{45}$$

$$-\nabla u \cdot \boldsymbol{n} = -\epsilon \nabla v \cdot \boldsymbol{n} = i_0 \sinh(v-u), \quad \text{on} \quad \partial\Omega_{ae},\ \partial\Omega_{ce}, \tag{46}$$

A similar potential system can be derived in the dilute-ion case, but there are compatibility conditions that must be satisfied if the potential system is to be equivalent to the concentration system derived in the previous section.

4 Steady State Homogenization for the Cathode

This section deals with the variational homogenization of the cathode, and presents exact bounds on the effective (homogenized) conductivity. Based on the non-dimensional potential system (44–46) above, one can derive a non-dimensional steady-state system by setting the time derivative in the solid electrode equal to a constant:

$$-\frac{\partial v}{\partial t} \quad = \quad g \tag{47}$$

where g is a non-dimensional constant source term; $g > 0$ in the cathode representing that the cathode is a source for Li^+ ions. This steady-state assumption is not appropriate when current first begins to flow (just after the battery is first put in a circuit), or near the end of the battery's life, but should be reasonable when the battery is providing essentially steady current at essentially constant potential. In this case, the solid cathode is a steady source for Li atoms to diffuse toward the cathode surface. Combining (44–46) and (47), one obtains a non-dimensional steady-state potential system:

$$0 = \nabla^2 u, \quad \text{in} \quad \Omega_e, \tag{48}$$

$$-\nabla \cdot (\epsilon \nabla v) = g, \quad \text{in} \quad \Omega_c, \tag{49}$$

$$-\nabla u \cdot \boldsymbol{n} = -\epsilon \nabla v \cdot \boldsymbol{n} = i_0 \sinh(v-u), \quad \text{on} \quad \partial\Omega_{ce}. \tag{50}$$

Again this system must be coupled with the same sorts of far-field conditions as in the previous sections.

Now let θ_s be the fraction of cathode composed of solid electrode, and $\theta_e := 1-\theta_s$, the electrolyte fraction. Studying composite materials, Lipton & Vernescu [5, 6] used a variational approach to the linearized case where $\sinh(v-u)$ is replaced by $v-u$. In this case they have shown that one can average over the cathode to obtain a single homogeneous equation for v defined on the entire cathode, not just the solid electrode:

$$\nabla \cdot (\kappa \nabla v) = \theta_s g, \qquad \text{in} \quad \text{Cathode} = \Omega_e \cup \partial\Omega_{ce} \cup \Omega_c \,. \tag{51}$$

Here κ is a non-dimensionalized effective (macro-scale) electrochemical conductivity. A similar equation hold for u again extended to the entire averaged cathode, not just the electrolyte. The principal significance of these averaged (homogenized) equations is that one can obtain rigorous bounds on the effective conductivity κ. In particular, Lipton & Vernescu find that

$$\left(\frac{1}{1-m_0} + \frac{1}{\theta_s c^*}\right)^{-1} \le \kappa \le \left(\frac{1}{\epsilon} + \frac{\theta_e i_0 \delta + \theta_s \lambda + \frac{2}{3}\epsilon}{i_0 \lambda \delta + \frac{2}{3}\theta_e \lambda \epsilon + \frac{2}{3}\theta_s \epsilon i_0 \delta}\right)^{-1} \tag{52}$$

where

$$\lambda := (1-1/\epsilon)^{-1}, \tag{53}$$

$$c^* := 1/i_0\delta - (1-1/\epsilon)\,, \tag{54}$$

and again δ is the typical dimensionless particle radius. The parameter m_0 is the effective conductivity for a cathode with the solid electrode particles replaced by nonconducting particles and an electrolyte having unit conductivity. This effective conductivity is the inverse of the *formation factor* in the porous media literature.

5 Asymptotic analysis

Here we consider one-dimensional problem based on the first dilute-ion model describing a planar cell in which the anode occupies the region $0 < x < 1$ while the cathode occupies the region $1 < x < \Lambda$ and is separated from the anode by a thin spacer. Furthermore we assume that the composition of the electrodes is isotropic so that $\mathcal{B}_{ij} = \mathcal{B}(x)\delta_{ij}$.

We base our asymptotic analysis of the model on the assumptions that $\lambda \gg 1$ and, in line with parameter estimates, consider the distinguished limit $\gamma = O(1)$, $\kappa_n = O(1)$, $\kappa_p = O(1)$, $\mathcal{V} = O(1)$, $\nu = O(\lambda)$ and $\Gamma = O(\lambda)$. In addition the other significant choice we have is that of γ which we take to be $O(1)$; from a physical point of view this corresponds to placing a very high load on the battery and so is a particularly interesting limit. Following the assumptions made about the sizes of the parameters Γ and ν we write

$$\Gamma = \lambda\tilde{\Gamma}, \qquad \nu = \lambda\tilde{\nu},$$

where $\tilde{\Gamma}$ and $\tilde{\nu}$ are $O(1)$ parameters.

We expand the variables as follows:

$$\begin{gathered} c = c_0(x,t) + \cdots\,, \qquad d_*\phi = \phi_0(t) + \tfrac{1}{\lambda}\phi_1(x,t) + \cdots\,, \quad \Phi = \Phi_0 + \cdots\,, \\ d_* c_s = c_{s,0} + \tfrac{1}{\lambda}c_{s,1} + \cdots\,, \qquad d_*\tilde{R} = \tilde{R}_0 + \cdots\,, \qquad \tilde{S} = \tilde{S}_0 + \cdots\,. \end{gathered} \tag{55}$$

The electrolyte. Substitution of the above expansion into (34) and (24) yields

$$\frac{\partial}{\partial x}\left(\mathcal{B}\frac{\partial c_0}{\partial x}\right) + \frac{1}{2p\gamma\kappa_p}(\tilde{R}_0 H(1-x) + \tilde{S}_0 H(x-1)) = 0, \tag{56}$$

$$\left.\frac{\partial c_0}{\partial x}\right|_{x=0} = 0, \qquad \left.\frac{\partial c_0}{\partial x}\right|_{x=\Lambda} = 0, \tag{57}$$

where $H(\cdot)$ is the Heaviside function. Since this is Neumann problem for c_0 we require an extra condition on c_0 in order to specify its magnitude. It is clear from (24) that lithium ions neither enter nor leave the system. Thus the average lithium ion concentration across the cell is independent of time. Assuming that c has been non-dimensionalized with this average concentration implies that

$$\int_0^\Lambda c_0 dx = \Lambda \tag{58}$$

Butler Volmer conditions. Substitution of the expansion (55) into the Butler-Volmer conditions (21d) and (23d) yields, to leading order,

$$\phi_0(t) = U(c_{s,0}|_{\partial\Omega_{ae}}), \qquad \Phi_0 = \phi_0(t) + V(c_{s,0}|_{\partial\Omega_{ce}}). \tag{59}$$

An important corollary of this result is that the concentration of lithium on the edge of the anode particles $c_{s,0}|_{\partial\Omega_{ae}}$ and the concentration of lithium on the edge of the cathode particles $c_{s,0}|_{\partial\Omega_{ae}}$ are both functions of time only being completely independent of the position of the particle within the electrode.

The electrode particles. The leading order terms in the expansion of (36)-(36) are

$$\hat{\nabla}^2 c_{s,0} = 0, \qquad \left.\frac{\partial c_{s,0}}{\partial n}\right|_{\partial\hat{\Omega}_{per}} = 0$$

in both anode and cathode particles. Solving the above gives

$$c_{s,0} = c_{a,0}(t) \qquad \text{in the anode,} \qquad c_{s,0} = c_{c,0}(t) \qquad \text{in the cathode.} \tag{60}$$

Proceeding to next order in the expansion of (36)-(36) we find

$$\frac{dc_{s,0}}{dt} = \tilde{\Gamma}\hat{\nabla}^2 c_{s,1}, \qquad \left.\frac{\partial c_{s,1}}{\partial n}\right|_{\partial\hat{\Omega}_{per}} = -Q_0$$

where $Q_0 = R_0$ in the anode and $Q_0 = S_0$ in the cathode. Integrating this over the particles contained within the periodic domain $\hat{\Omega}_{per}$ yields

$$|\hat{\Omega}_{per}|\frac{dc_{s,0}}{dt} = -\tilde{\Gamma}\int_{\partial\hat{\Omega}_{per}} Q_0 d\hat{S} = -\tilde{\Gamma}\tilde{Q}_0,$$

where $|\hat{\Omega}_{per}| = \int_{\hat{\Omega}_{per}} d\hat{V}$. By substituting this expression into leading order expansion of (80) we obtain the following expressions for the rate of change of lithium ion concentration in the electrodes and for the averaged reaction rates

$$\begin{aligned} &d_*\tfrac{dc_{a,0}}{dt} = -Ip\tilde{\Gamma}\left(\int_0^1 \tfrac{|\hat{\Omega}_{per}|}{\mathcal{V}+|\hat{\Omega}_{per}|}dx\right)^{-1}, \qquad d_*\tfrac{dc_{c,0}}{dt} = Ip\tilde{\Gamma}\left(\int_1^\Lambda \tfrac{|\hat{\Omega}_{per}|}{\mathcal{V}+|\hat{\Omega}_{per}|}dx\right)^{-1}, \\ &d_*\tilde{R}_0 = Ip|\hat{\Omega}_{per}|\left(\int_0^1 \tfrac{|\hat{\Omega}_{per}|}{\mathcal{V}+|\hat{\Omega}_{per}|}dx\right)^{-1}, \quad d_*\tilde{S}_0 = -Ip|\hat{\Omega}_{per}|\left(\int_1^\Lambda \tfrac{|\hat{\Omega}_{per}|}{\mathcal{V}+|\hat{\Omega}_{per}|}dx\right)^{-1}, \end{aligned} \tag{61}$$

Summary of the simplified model. The resulting leading order model is comprised of equations (56), (57), (58), (59) and (61) which, on dropping subscripts and substituting R or S as appropriate for Q, can be written as

$$d_*\frac{dc_a}{dt} = -Ip\tilde{\Gamma}\left(\int_0^1 \frac{|\hat{\Omega}_{per}|}{\mathcal{V}+|\hat{\Omega}_{per}|}dx\right)^{-1}, \qquad d_*\frac{dc_c}{dt} = Ip\tilde{\Gamma}\left(\int_1^\Lambda \frac{|\hat{\Omega}_{per}|}{\mathcal{V}+|\hat{\Omega}_{per}|}dx\right)^{-1}, \tag{62}$$

$$\phi(t) = U(c_a), \qquad \Phi = \phi(t) + V(c_c), \tag{63}$$

and

$$\frac{\partial}{\partial x}\left(\mathcal{B}\frac{\partial c}{\partial x}\right) + \frac{1}{2p\gamma\kappa_p}\left(\tilde{R}H(1-x)+\tilde{S}H(x-1)\right) = 0, \tag{64}$$

$$\left.\frac{\partial c}{\partial x}\right|_{x=0} = 0, \qquad \left.\frac{\partial c}{\partial x}\right|_{x=\Lambda} = 0, \qquad \int_0^\Lambda c dx = \Lambda, \tag{65}$$

$$d_*\tilde{R} = Ip|\hat{\Omega}_{per}|\left(\int_0^1 \frac{|\hat{\Omega}_{per}|}{\mathcal{V}+|\hat{\Omega}_{per}|}dx\right)^{-1}, \qquad d_*\tilde{S} = -Ip|\hat{\Omega}_{per}|\left(\int_1^\Lambda \frac{|\hat{\Omega}_{per}|}{\mathcal{V}+|\hat{\Omega}_{per}|}dx\right)^{-1}. \tag{66}$$

Note that $\int_0^\Lambda \tilde{R}H(1-x)+\tilde{S}H(x-1)dx = 0$ (since $\mathcal{V}+|\hat{\Omega}_{per}|$ is constant throughout the entire cell) and hence that a solution to (64)-(66) exists. If the battery is being charged then typically I is specified. If, on the other hand, it is being used to power a device then it will be related to the total potential drop across the cell by, for example, Ohm's law

$$\Phi = I\omega, \tag{67}$$

where ω is the resistance of the device.

From a practical point of view the desired outputs of the model are the current I (where this is not specified) and the potential drop across the cell Φ. These may be obtained from solving (62)-(63) and (67). The importance of the remaining equations (64)-(66) may therefore be questioned. However these still need to be solved in order to check whether the solution for c passes through zero. If it does the asymptotic expansion is invalid in at least some region of the cell; physically this corresponds to a high power demand on the cell causing lithium ion concentration to decrease to zero, leading to a break in the current flowing through the electrolyte and hence failure of the cell.

6 Computations with Two-Dimensional Anode Geometries

In this section we describe an atomistic approach to modelling certain aspects of the lithium ion battery system. In particular, we focus here only on the anode region of the battery and further allow only diffusion of lithium in the solid particles and ionization of lithium at the particle/electrolyte interface. Diffusion and advection of lithium ions in the electrolyte are assumed to occur on a fast time scale such that lithium ions entering the electrolyte are instantaneously swept away. The numerical calculations do incorporate certain two-dimensional features of the anode geometry by allowing for the specification of a given packing fraction and a particle size distribution. Given such a distribution of particles, a Kinetic Monte Carlo (KMC) algorithm is implemented to model diffusion of lithium in the solid particles and ionization of lithium at the particle/electrolyte interface.

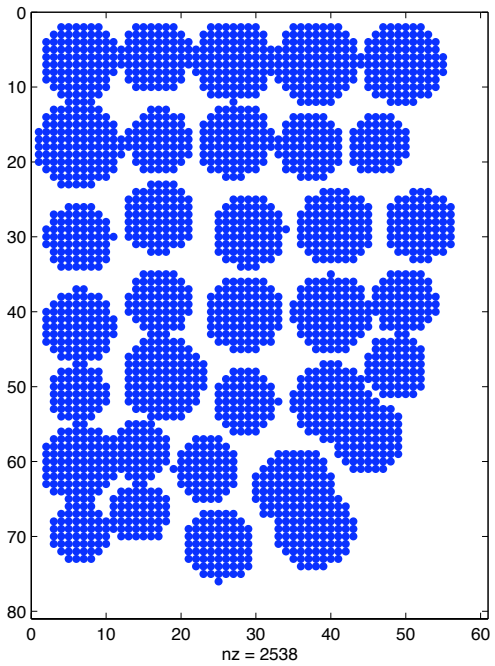

Figure 4: This figure shows an initial configuration of the electrode particle distribution in the anode in which all sites in each particle are filled with lithium atoms.

The numerical calculations set up a packing of particles in the anode in which the particle sizes are normally distributed. An example is shown in Figure 4. Lithium atoms are assumed to occupy points on a grid (80×60 in this example) that fall within the prescribed particles.

The above configuration of lithium atoms is then used as the initial condition for a Kinetic Monte Carlo scheme in which the lithium atoms diffuse in the solid and undergo reaction at the particle/electrolyte boundaries at generic 'hopping' rates R_j defined by the following expression

$$R_j \quad = \quad k_T \exp\left[-\frac{E_j}{k_B T}\right], \tag{68}$$

where k_T is a rate constant, k_B is the Boltzmann constant and T is the temperature. This basic approach was developed based on ideas outlined in Voter[12] and Schulze[9, 10]. In the present situation, we identify a finite number of events associated with the different rates R_j determined by different neighborhood configurations. In particular, we define

$$\begin{gathered} E_1 = E_B, \quad E_2 = E_B + E_n, \quad E_3 = E_B + 2E_n, \quad E_4 = E_B + 3E_n \\ E_5 = E_B + E_n^+, \quad E_6 = E_B + E_n + E_n^+, \quad E_7 = E_B + 2E_n + E_n^+, \quad E_8 = E_B + 3E_n + E_n^+, \end{gathered} \tag{69}$$

where E_B is an energy barrier present at each grid location, E_n is the energy associated with each lateral nearest neighbor in the solid particle and E_n^+ is the energy associated with the ionization of a lithium atom at the particle/electrolyte interface. For example, E_3 represents the energy barrier associated with the motion of a lithium atom with two lateral nearest neighbors from one point

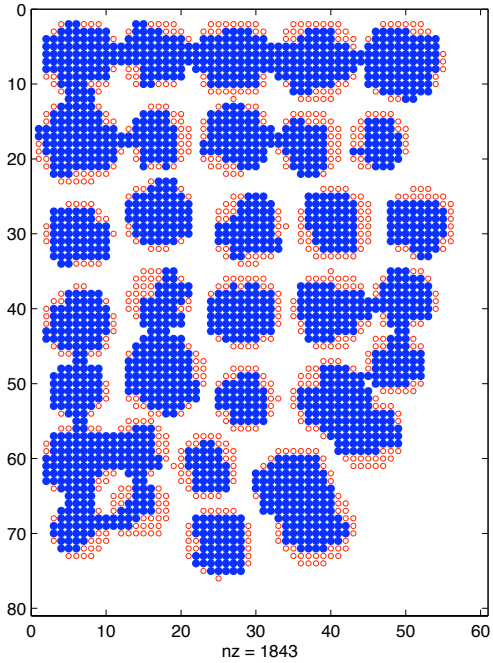

Figure 5: This figure shows the configuration of the particles in the anode after diffusion of lithium in the solid and has begun and ionized lithium is released into the surrounding electrolyte. Solid (blue) circles indicate the presence of lithium and open (red) circles indicate the location where lithium has diffused away. Diffusion of lithium in the particles and ionization at the particle/electrolyte boundaries are assumed to occur at rates based on nearest-neighbor interactions and known reaction rates.

in the solid particle to an adjacent point in the solid. Similarly, E_8 represents the energy barrier associated with the ionization of a lithium atom in the solid particle with three nearest neighbors into the electrolyte. While in principle one could undergo a study to relate the values E_B, E_n and E_n^+ to known diffusion coefficients and reaction rates, we have not made an attempt to do so here. Rather we have simply specified values for E_B, E_n and E_n^+ in order to assess this approach as a possible means of a more in depth study of this problem. To be sure, one would need to incorporate at a minimum transport effects of the lithium ions in the electrolyte and event rates that in a relative sense represent the different diffusion and ionization rates of lithium in order capture quantitative aspects of the anode.

We have implemented a basic KMC algorithm to execute an 'event' following the work of Voter[12] and Schulze[9]. For example, an event could be a lithium atom with no nearest neighbors in the solid hopping from one site in the solid to another site in the solid, or a lithium atom at the particle boundary with one nearest neighbor in the solid ionizing and 'hopping' into the electrolyte). An example of the particle anode system after the execution of 10000 events is shown in Figure 5.

The above two-dimensional atomistic approach to the lithium ion battery problem should be viewed as a potential starting point for the study of effects such as particle geometry and packing,

diffusion and reaction in the particles. This approach further may provide a means to incorporate other critical features of the model such as those related to the porous spacer, the cathode and three-dimensional effects.

7 Conclusion

We formulated two detailed models for an electrolytic cell with particulate electrodes based on a lithium atom concentration dependent Butler-Volmer condition at the interface between electrode particles and the electrolyte. The first was based on a dilute-ion assumption for the electrolyte, while the second assumed that Li ions are present in excess. For the first, we used the method of multiple scales to homogenize this model over the microstructure, formed by the small lithium particles in the electrodes. For the second, we gave rigorous bounds for the effective electrochemical conductivity for a linearized case. We expect similar results and bounds for the full nonlinear problem (48–50) because variational results are generally not adversely affected by a sinh term.

Finally we used the asymptotic methods, based on parameters estimated from the literature, to attain a greatly simplified one-dimensional version of the original homogenized model. This simplified model accounts for the fact that diffusion of lithium atoms within individual electrode particles is relatively much faster than that of lithium ions across the whole cell so that lithium ion diffusion is what limits the performance of the battery. However, since most of the potential drop occurs across the Debye layers surrounding each electrode particle, lithium ion diffusion only significantly affects cell performance if there is more or less complete depletion of lithium ions in some region of the electrolyte which causes a break in the current flowing across the cell. This causes catastrophic failure. Providing such failure does not occur the potential drop across the cell is determined by the concentration of lithium atoms in the electrode particles. Within each electrode lithium atom concentration is, to leading order, a function of time only and not of position within the electrode. The depletion of electrode lithium atom concentration is directly proportional to the current being drawn off the cell. This leads one to expect that the potential of the cell gradually drops as current is drawn of it.

We would like to emphasize that all the homogenization methods employed in this work give a systematic approach for investigating the effect that changes in the microstructure have on the behaviour of the battery. However, due to lack of time, we have not used this method to investigate particular particle geometries.

We would also like to point out possible extensions to the model. The most important of these is to investigate effects arising from changes in electrode particle size or geometry which occur as a result of depletion/accretion of lithium atoms. Another extension to this work is to carry out the homogenization of the potential and the lithium ion concentration in the spacer.

References

[1] J.D. Fehribach, Diffusion-reaction-conduction processes in porous electrodes: the electrolyte wedge problem, *European J. Appl. Math.* **12** (2001) 77–96.

[2] J.D. Fehribach & R. O'Hayre, Triple phase boundaries in solid-oxide cathodes, *SIAM J. Appl. Math.* **70** (2009), to appear.

[3] T.F. Fuller, M. Doyle & J. Newman, Simulation and optimisation of the dual lithium ion insertion cell. *J. Electrochem. Soc.* **141** (2000) 1–10.

[4] R.A. Huggins, Lithium alloy negative electrodes, *J. Power Sources* **81-82** (1999) 13–19.

[5] R. Lipton & B. Vernescu, Critical radius, size effects and inverse problems for composites with imperfect interfaces, *J. Appl. Phys.* **79** (1996) 8964–8966.

[6] R. Lipton & B. Vernescu, Composites with imperfect interface, *Proc. R. Soc. Lond. A* **452** (1996) 329–358.

[7] J.S. Newman, *Electrochemical Systems*, 2nd ed., Prentice Hall, Englewood Cliffs, NJ, 1991.

[8] G. Richardson & J.R. King, Time-dependent modelling and asymptotic analysis of electrochemical cells, *J. Eng. Math.* **59** (2007) 239–275.

[9] T.P. Schulze, Kinetic Monte Carlo simulations with minimal searching. *Phys. Rev. E* **65** (2002) 036704.

[10] T.P. Schulze, Morphological instability during directional epitaxy. *J. Crystal Growth* **295** (2006) 188–201.

[11] K. Tanaka & M. Nomura, Measurement of tracer diffusion coefficients of lithium ions, chloride ions and water in aqueous lithium chloride solutions, *J. Chem. Soc., Faraday Trans. 1* **83** (1987) 1779–1782.

[12] Voter, A.F. Introduction to the kinetic Monte Carlo method. In *Radiation Effects in Solids*, edited by K.E. Sickafus and E.A. Kotmin (Springer, NATO Publishing Unit, Dordrecht, The Netherlands, 2005).

A Derivation of the averaged diffusion equation with sources.

In this section we consider how we can derive averaged equations, over the lengthscale of the electrode, for the processes occurring in the electrolyte where the electrolyte has a micro structure. In this instance we take the lengthscale of the microstructure to be of $O(\epsilon)$ and that of the electrode to be of $O(1)$ where $\epsilon \ll 1$. Furthermore we assume that the microstructure is *locally* periodic inside a completely periodic array of boxes which we denote by $\hat{V}_{per} \cup \hat{\Omega}_{per}$. Here $\hat{V}_{per}$ represents the space inside this box occupied by the electrolyte while $\hat{\Omega}_{per}$ represents the space occupied by the electrode (see figure 6 for an example configuration). For the sake of generality we allow the microstructure to change slowly, over the $O(1)$ lengthscale, and it is in this sense that it is *locally* periodic.

Consider the following dimensionless equations for c and ϕ which both satisfy Neumann boundary condition on the microstructured boundary $\partial\hat{\Omega}_{per}$

$$\frac{\partial c}{\partial t} + \nabla \cdot \boldsymbol{q} = 0, \qquad \text{where} \quad \boldsymbol{q} = -D\nabla c, \tag{70}$$

$$\boldsymbol{q} \cdot \boldsymbol{n}|_{\partial\hat{\Omega}_{per}} = \epsilon k Q, \tag{71}$$

$$\nabla \cdot \boldsymbol{f} = 0 \qquad \text{where} \quad \boldsymbol{f} = -D(\lambda c \nabla\phi - \alpha\nabla c), \tag{72}$$

$$\boldsymbol{f} \cdot \boldsymbol{n}|_{\partial\hat{\Omega}_{per}} = \epsilon k(1-\alpha) Q, \tag{73}$$

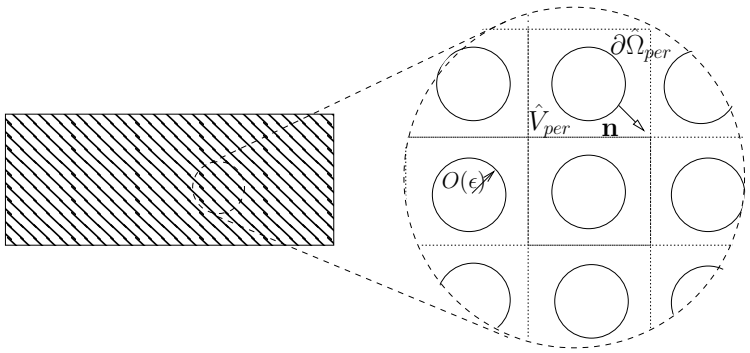

Figure 6: Illustration of the microstructured boundary.

Here $\boldsymbol{n}$ is the unit outward normal to $\hat{\Omega}_{per}$ or equivalently the unit inward normal to $\hat{V}_{per}$ (see figure 6).

Multiple scales formulation. We investigate the distinguished limit that k, D and Q are $O(1)$ while $\epsilon \ll 1$ by introducing the microscale variable $\hat{\boldsymbol{x}}$ defined by

$$\boldsymbol{x} = \epsilon\hat{\boldsymbol{x}}.$$

In terms of this new variable the multiple scales expansion of the operator ∇ takes the form $\nabla = \nabla + \hat{\nabla}/\epsilon$. We can thus rewrite (70)-(72) in the form

$$\frac{\partial c}{\partial t} + \frac{1}{\epsilon}\hat{\nabla}\cdot\boldsymbol{q} + \nabla\cdot\boldsymbol{q} = 0, \qquad \boldsymbol{q} = -D\left(\frac{1}{\epsilon}\hat{\nabla}c + \nabla c\right), \tag{74}$$

$$\boldsymbol{q}\cdot\boldsymbol{n}|_{\partial\hat{\Omega}_{per}} = -\epsilon Q, \qquad c \quad \text{periodic in } \hat{\boldsymbol{x}} \text{ on} \quad \hat{V}_{per}, \tag{75}$$

$$\frac{1}{\epsilon}\hat{\nabla}\cdot\boldsymbol{f} + \nabla\cdot\boldsymbol{f} = 0, \qquad \boldsymbol{f} = -D\left[\left(\frac{1}{\epsilon}\lambda c\hat{\nabla}\phi + \lambda c\nabla\phi\right) - \alpha\left(\frac{1}{\epsilon}\hat{\nabla}c + \nabla c\right)\right], \tag{76}$$

$$\boldsymbol{f}\cdot\boldsymbol{n}|_{\partial\hat{\Omega}_{per}} = \epsilon kQ(1-\alpha), \qquad \phi \quad \text{periodic in } \hat{\boldsymbol{x}} \text{ on} \quad \hat{V}_{per}, \tag{77}$$

Mathematical preliminary. Before proceeding with the expansion we re-emphasize that although the interface $\partial\hat{\Omega}_{per}$ is approximately periodic on the short lengthscale significant variations can occur over the longer $\boldsymbol{x}$ lengthscale. We will find it useful to define this interface by the zero level set of the function ψ, that is by the relation $\psi(\hat{\boldsymbol{x}}, \boldsymbol{x}) = 0$. Furthermore we define ψ so that $\boldsymbol{n}$, the outward unit normal to $\hat{\Omega}_{per}$, (or equivalently the unit inward normal to $\hat{V}_{per}$) is given by

$$\boldsymbol{n} = -\frac{\hat{\nabla}\psi + \epsilon\nabla\psi}{|\hat{\nabla}\psi + \epsilon\nabla\psi|}. \tag{78}$$

We are then able to calculate the rate of change of a quantity $A(\hat{\boldsymbol{x}}, \boldsymbol{x})$ integrated over the locally periodic domain $\hat{V}_{per}$ in terms of the surface function ψ (see §A.1) finding it to be

$$\frac{\partial}{\partial x_i}\int_{\hat{V}_{per}} A(\hat{\boldsymbol{x}}, \boldsymbol{x})d\hat{V} \sim \int_{\hat{V}_{per}} \frac{\partial A}{\partial x_i}d\hat{V} - \int_{\partial\hat{\Omega}_{per}} A\frac{1}{|\hat{\nabla}\psi|}\frac{\partial\psi}{\partial x_i}d\hat{S}.$$

In turn we can use the above result to show that

$$\nabla \cdot \int_{\hat{V}_{per}} \boldsymbol{q}(\hat{\boldsymbol{x}}, \boldsymbol{x}) d\hat{V} \sim \int_{\hat{V}_{per}} \nabla \cdot \boldsymbol{q} d\hat{V} - \int_{\partial\hat{\Omega}_{per}} A \frac{\boldsymbol{q} \cdot \nabla\psi}{|\hat{\nabla}\psi|} d\hat{S}. \tag{79}$$

The asymptotic expansion. We now expand the variables in (74)-(77) as follows:

$$\begin{aligned}
c &= c_0(\boldsymbol{x}, t) + \epsilon c_1(\hat{\boldsymbol{x}}, \boldsymbol{x}, t) + \epsilon^2 c_2(\hat{\boldsymbol{x}}, \boldsymbol{x}\, t) + \cdots, \\
\phi &= \frac{1}{\lambda}\left(\phi_0(\boldsymbol{x}, t) + \epsilon\phi_1(\hat{\boldsymbol{x}}, \boldsymbol{x}, t) + \epsilon^2\phi_2(\hat{\boldsymbol{x}}, \boldsymbol{x}\, t) + \cdots\right), \\
\boldsymbol{q} &= \boldsymbol{q}_0(\hat{\boldsymbol{x}}, \boldsymbol{x}, t) + \epsilon\boldsymbol{q}_1(\hat{\boldsymbol{x}}, \boldsymbol{x}, t) + \epsilon^2\boldsymbol{q}_2(\hat{\boldsymbol{x}}, \boldsymbol{x}, t) + \cdots, \\
\boldsymbol{f} &= \boldsymbol{f}_0(\hat{\boldsymbol{x}}, \boldsymbol{x}, t) + \epsilon\boldsymbol{f}_1(\hat{\boldsymbol{x}}, \boldsymbol{x}, t) + \epsilon^2\boldsymbol{f}_2(\hat{\boldsymbol{x}}, \boldsymbol{x}, t) + \cdots.
\end{aligned}$$

Derivation of a solvability condition on c_0. Consider first the flux equations for $\boldsymbol{q}$ (74)-(75). To leading order we obtain

$$\hat{\nabla} \cdot \boldsymbol{q}_0 = 0, \qquad \boldsymbol{q}_0 \cdot \boldsymbol{n}|_{\partial\hat{\Omega}_{per}} = 0, \qquad \boldsymbol{q}_0 \quad \text{periodic in } \hat{\boldsymbol{x}} \text{ on } \hat{V}_{per}. \tag{80}$$

At $O(\epsilon)$ in (74)-(75) we find

$$\frac{\partial c_0}{\partial t} + \hat{\nabla} \cdot \boldsymbol{q}_1 + \nabla \cdot \boldsymbol{q}_0 = 0, \qquad \boldsymbol{q}_1 \quad \text{periodic in } \hat{\boldsymbol{x}} \text{ on } \hat{V}_{per}, \quad \boldsymbol{q}_1 \cdot \boldsymbol{n}|_{\partial\hat{\Omega}_{per}} = kQ,$$

Rewriting the boundary condition (81) in terms of the surface function $\psi(\hat{\boldsymbol{x}}, \boldsymbol{x})$ (recalling that the normal to $\partial\Omega$ is given by (78)) gives

$$\boldsymbol{q}_1 \cdot \hat{\nabla}\psi + \boldsymbol{q}_0 \cdot \nabla\psi|_{\partial\hat{\Omega}_{per}} = -|\hat{\nabla}\psi| kQ. \tag{81}$$

Integrating (81) over $\hat{V}_{per}$ and using the fact the *outward* normal to $\hat{V}_{per}$ on that section of the boundary it shares with $\hat{\Omega}_{per}$ is, to leading order in ϵ, $\hat{\nabla}\psi/|\hat{\nabla}\psi|$ results in the integral equations

$$\int_{\hat{V}_{per}} \frac{\partial c_0}{\partial t} + \nabla \cdot \boldsymbol{q}_0 d\hat{V} + \int_{\hat{\Omega}_{per}} \boldsymbol{q}_1 \cdot \frac{\hat{\nabla}\psi}{|\hat{\nabla}\psi|} d\hat{S} = 0,$$

which in turn, on substitution of (81) gives

$$\int_{\hat{V}_{per}} \frac{\partial c_0}{\partial t} + \nabla \cdot \boldsymbol{q}_0 d\hat{V} - \int_{\hat{\Omega}_{per}} \boldsymbol{q}_0 \cdot \frac{\nabla\psi}{|\hat{\nabla}\psi|} d\hat{S} = \int_{\hat{\Omega}_{per}} kQ d\hat{S},$$

Finally, we use the result (79) to rewrite this in the desired form

$$\int_{\hat{V}_{per}} \frac{\partial c_0}{\partial t} d\hat{V} + \nabla \cdot \int_{\hat{V}_{per}} \boldsymbol{q}_0 d\hat{V} = \int_{\hat{\Omega}_{per}} kQ d\hat{S}, \tag{82}$$

It remains to determine $\boldsymbol{q}_0$ in terms of c_0. To leading order in (74b) we find

$$\boldsymbol{q}_0 = -D(\nabla c_0 + \hat{\nabla} c_1).$$

Substitution of this into (80) yields

$$\hat{\nabla}^2 c_1 = 0, \qquad \boldsymbol{n}\cdot\hat{\nabla}c_1|_{\partial\hat{\Omega}_{per}} = -\boldsymbol{n}\cdot\nabla c_0|_{\partial\hat{\Omega}_{per}}, \qquad c_1 \quad \text{periodic in } \hat{\boldsymbol{x}} \text{ on } \hat{V}_{per}.$$

We make use of the linearity of this problem to write its solution in the form

$$c_1 = -\left(\frac{\partial c_0}{\partial x_1}\chi^{(1)}(\hat{\boldsymbol{x}},\boldsymbol{x}) + \frac{\partial c_0}{\partial x_2}\chi^{(2)}(\hat{\boldsymbol{x}},\boldsymbol{x}) + \frac{\partial c_0}{\partial x_3}\chi^{(3)}(\hat{\boldsymbol{x}},\boldsymbol{x})\right), \tag{83}$$

where the basis functions $\chi^{(i)}$ satisfy the following problems:

$$\left.\begin{array}{c} \hat{\nabla}^2\chi^{(i)} = 0, \\ \hat{\nabla}\chi^{(i)}\cdot\boldsymbol{n}|_{\partial\hat{\Omega}_{per}} = \boldsymbol{e}_i\cdot\boldsymbol{n}|_{\partial\hat{\Omega}_{per}}, \\ \chi^{(i)} \quad \text{periodic in } \hat{\boldsymbol{x}} \text{ on } \quad \hat{V}_{per}, \\ \int_{\hat{V}_{per}}\chi^{(i)}d\hat{V} = 0 \end{array}\right\} \quad \text{for} \quad i = 1,2,3 \tag{84}$$

and $\boldsymbol{e}_i$ is a basis vector in the x_i-direction. It follows that the leading order flux is given by

$$\boldsymbol{q}_0 = -D\left(\delta_{ij} - \frac{\partial\chi^{(j)}}{\partial\hat{x}_i}\right)\frac{\partial c_0}{\partial x_j}\boldsymbol{e}_i.$$

where the Einstein summation convention is used. Substitution of this result into (82) then yields an equation for c_0 in terms of the macroscopic variable $\boldsymbol{x}$

$$\boxed{\mathcal{V}\frac{\partial c_0}{\partial t} = D\frac{\partial}{\partial x_i}\left(\mathcal{B}_{ij}\frac{\partial c_0}{\partial x_j}\right) + k\tilde{Q},} \tag{85}$$

where

$$\mathcal{V} = \int_{\hat{V}_{per}} d\hat{V}, \qquad \mathcal{B}_{ij} = \left(\mathcal{V}\delta_{ij} - \int_{\hat{V}_{per}}\frac{\partial\chi^{(j)}}{\partial\hat{x}_i}\right), \qquad \tilde{Q} = \int_{\partial\hat{\Omega}_{per}} Q d\hat{S} \tag{86}$$

Derivation of a solvability condition on ϕ_0. The derivation of the solvability condition for ϕ_0 proceeds along very similar lines to that for c_0. At leading order in the flux equations for $\boldsymbol{f}$, namely (76) we find

$$\hat{\nabla}\cdot\boldsymbol{f}_0 = 0, \qquad \boldsymbol{f}_0\cdot\boldsymbol{n}|_{\partial\hat{\Omega}_{per}} = 0, \qquad \boldsymbol{f}_0 \quad \text{periodic in } \hat{\boldsymbol{x}} \text{ on } \hat{V}_{per}. \tag{87}$$

At next order we find an equation for $\boldsymbol{f}_1$ which we can integrate in a similar manner to that for $\boldsymbol{q}_1$ in order to obtain the following solvability condition on $\boldsymbol{f}_0$:

$$\nabla\cdot\int_{\hat{V}_{per}}\boldsymbol{f}_0 d\hat{V} = k(1-\alpha)\int_{\partial\hat{\Omega}_{per}} Q d\hat{S}. \tag{88}$$

Substituting the expansions for c and ϕ into (76b) gives the following expression for $\boldsymbol{f}_0$:

$$\boldsymbol{f}_0 = -D\left(c_0\hat{\nabla}\phi_1 - \alpha\hat{\nabla}c_1 + c_0\nabla\phi_0 - \alpha\nabla c_0\right).$$

In turn substitution of this expression into (87) yields a system for ϕ_1

$$\hat{\nabla}^2\phi_1 = 0, \qquad \hat{\nabla}\phi_1 \cdot \boldsymbol{n}|_{\partial\hat{\Omega}_{per}} = -\nabla\phi_0 \cdot \boldsymbol{n}|_{\partial\hat{\Omega}_{per}},$$

with solution

$$\phi_1 = -\left(\frac{\partial\phi_0}{\partial x_1}\chi^{(1)}(\hat{\boldsymbol{x}}, \boldsymbol{x}) + \frac{\partial\phi_0}{\partial x_2}\chi^{(2)}(\hat{\boldsymbol{x}}, \boldsymbol{x}) + \frac{\partial\phi_0}{\partial x_3}\chi^{(3)}(\hat{\boldsymbol{x}}, \boldsymbol{x})\right), \tag{89}$$

from which it follows that

$$\boldsymbol{f}_0 = -D\left(\delta_{ij} - \frac{\partial\chi^{(j)}}{\partial\hat{x}_i}\right)\left(c_0\frac{\partial\phi_0}{\partial x_j} - \alpha\frac{\partial c_0}{\partial x_j}\right)\boldsymbol{e}_i.$$

On substitution of this expression into (88) we obtain an equation for ϕ_0

$$\boxed{D\frac{\partial}{\partial x_i}\left(\mathcal{B}_{ij}\left(c_0\frac{\partial\phi_0}{\partial x_j} - \alpha\frac{\partial c_0}{\partial x_j}\right)\right) + k(1-\alpha)\tilde{Q} = 0.} \tag{90}$$

Notably the macroscale equations (85) and (90) we have derived for c_0 and ϕ_0, respectively, are both in conservation from.

A.1 Rate of change of integrated quantities

Consider the surface $\partial\hat{\Omega}_{per}$ defined by $\psi(\hat{\boldsymbol{x}}, \boldsymbol{x}) = 0$. Alternatively we can write this in the form $\hat{\boldsymbol{x}} = \boldsymbol{r}(\tau_1, \tau_2, \boldsymbol{x})$ so that $\psi(\boldsymbol{r}, \boldsymbol{x}) = 0$. Since $\psi(\boldsymbol{r} + d\boldsymbol{r}, \boldsymbol{x} + dx_i\boldsymbol{e}_i) = 0$ it follows that

$$\frac{\partial\boldsymbol{r}}{\partial x_i} \cdot \hat{\nabla}\psi = -\frac{\partial\psi}{\partial x_i}.$$

By using the fact that the unit inward normal to $\hat{V}_{per}$ is defined, in terms of ψ, by $\boldsymbol{n} = -\hat{\nabla}\psi/|\hat{\nabla}\psi| + O(\epsilon)$ we can rewrite the above in the form

$$\frac{\partial\boldsymbol{r}}{\partial x_i} \cdot \boldsymbol{n} = \frac{1}{|\hat{\nabla}\psi|}\frac{\partial\psi}{\partial x_i} + O(\epsilon), \tag{91}$$

(see figure 7 for an illustration on this). We can identify the quantity $dx_i\frac{\partial\boldsymbol{r}}{\partial x_i} \cdot \boldsymbol{n}$ as the normal distance between the surface $\partial\hat{\Omega}_{per}$ at $\boldsymbol{x}$ and $\partial\hat{\Omega}_{per}$ at $\boldsymbol{x} + dx_i\boldsymbol{e}_i$. The rate of change of $\int_{\hat{V}_{per}} A(\hat{\boldsymbol{x}}, \boldsymbol{x})d\hat{V}$ is thus comprised of two terms, the first representing the rate of change of A with x_i and the second arising from the rate of change of the boundary to V with x_i which can be written as the surface integral

$$-\int_{\partial\hat{\Omega}_{per}} A\frac{\partial\boldsymbol{r}}{\partial x_i} \cdot \boldsymbol{n}d\hat{S}$$

It follows that

$$\frac{\partial}{\partial x_i}\int_{\hat{V}_{per}} A(\hat{\boldsymbol{x}}, \boldsymbol{x})d\hat{V} \sim \int_{\hat{V}_{per}} \frac{\partial A}{\partial x_i}d\hat{V} - \int_{\partial\hat{\Omega}_{per}} A\frac{1}{|\hat{\nabla}\psi|}\frac{\partial\psi}{\partial x_i}d\hat{S}.$$

Here the first term on the right-hand side represents the change in A with x_i while the second term arises because the domain $\hat{V}_{per}$ changes

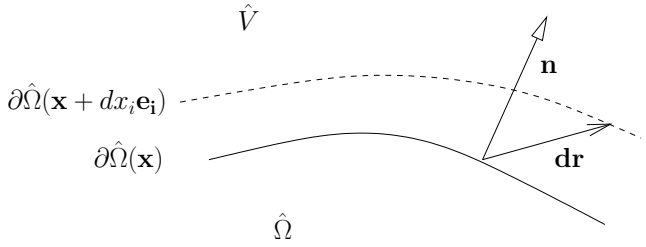

Figure 7: Illustration of the microstructured boundary.

A.2 Useful Results

There are a number of results which help illustrate the behaviour of the tensor $\mathcal{B}_{ij}$. The most of important of these are

$$\int_{\hat{V}_{per}} \frac{\partial \chi^{(j)}}{\partial \hat{x}_i} d\hat{V} = -\int_{\partial\hat{\Omega}_{per}} \chi^{(j)} \boldsymbol{e}_i \cdot \boldsymbol{n} d\hat{S}, \tag{92}$$

$$\int_{\hat{V}_{per}} \frac{\partial \chi^{(j)}}{\partial \hat{x}_i} d\hat{V} = \int_{\hat{V}_{per}} \frac{\partial \chi^{(i)}}{\partial \hat{x}_j} d\hat{V}, \tag{93}$$

$$\int_{\hat{V}_{per}} \frac{\partial \chi^{(i)}}{\partial \hat{x}_i} d\hat{V} > 0 \qquad \text{(no summation)}. \tag{94}$$

The first of these results can be demonstrated by a straightforward application of the divergence theorem; the proofs for the second and third result are given below.

We can use results (93)-(94) to show that

$$\mathcal{B}_{ij} = \mathcal{B}_{ji}, \qquad \mathcal{B}_{ii} < 1. \qquad \text{(no summation)}. \tag{95}$$

Thus the tensor $\mathcal{B}_{ij}$ is symmetric and furthermore the effective diffusivity in any particular direction is reduced by the microstructure below that which would be observed without microstructure (which is precisely what one expects). In particular, for a uniform isotropic microstructure we have (as previously stated) $\mathcal{B}_{ij} = \mathcal{B}\delta_{ij}$ with $\mathcal{B} > 0$. It follows that the effective diffusivity $D\mathcal{B}$ is smaller than the diffusivity D in the absence of microstructure.

Proof of (93). Consider the integral I defined by

$$I = \int_{\hat{V}_{per}} \hat{\nabla} \cdot \left(\chi^{(i)} \hat{\nabla} \chi^{(k)} - \chi^{(k)} \hat{\nabla} \chi^{(i)} \right) d\hat{V} = \int_{\hat{V}_{per}} (\chi^{(i)} \hat{\nabla}^2 \chi^{(k)} - \chi^{(k)} \hat{\nabla}^2 \chi^{(i)}) d\hat{V}$$

It follows from the definition of $\chi^{(i)}$ (see (84)) that $I = 0$. If we now apply the divergence theorem to I we find that

$$I = -\int_{\partial\hat{\Omega}_{per}} \left(\chi^{(i)} \hat{\nabla} \chi^{(k)} - \chi^{(k)} \hat{\nabla} \chi^{(i)} \right) \cdot \boldsymbol{n} d\hat{S}.$$

Referring to the boundary conditions on $\chi^{(i)}$ on $\partial\hat{\Omega}_{per}$ contained in (84) and using the fact that $I = 0$ leads to the result

$$\int_{\partial\hat{\Omega}_{per}} \chi^{(k)} \boldsymbol{e}_i \cdot \boldsymbol{n} d\hat{S} = \int_{\partial\hat{\Omega}_{per}} \chi^{(i)} \boldsymbol{e}_k \cdot \boldsymbol{n} d\hat{S},$$

and hence by the result (92) to the desired result, namely (93).

Proof of (94). We can readily show that

$$-\int_{\partial\hat{\Omega}_{per}} \chi^{(i)} \boldsymbol{e}_i \cdot \boldsymbol{n} d\hat{S} > 0$$

and thus that the trace of the diffusivity tensor is increased by the microstructure, as might be expected. In order to see this consider multiplying (84) by $\chi^{(i)}$ to show that

$$\left.\begin{array}{c} \hat{\nabla} \cdot (\chi^{(i)} \hat{\nabla} \chi^{(i)}) = |\hat{\nabla} \chi^{(i)}|^2 \\ \chi^{(i)} \hat{\nabla} \chi^{(i)} \cdot \boldsymbol{n}|_{\partial\hat{\Omega}_{per}} = \chi^{(i)} \boldsymbol{e}_i \cdot \boldsymbol{n}|_{\partial\hat{\Omega}_{per}} \\ \chi^{(i)} \hat{\nabla} \chi^{(i)} \quad \text{periodic in } \hat{\boldsymbol{x}} \text{ on } \quad \hat{V}_{per} \end{array}\right\} \quad \text{for} \quad i = 1, 2, 3 \tag{96}$$

Integrating the first of these equations over V gives

$$\int_{\hat{V}_{per}} |\hat{\nabla} \chi^{(i)}|^2 d\hat{V} = \int_{\partial V \setminus \partial\hat{\Omega}_{per}} \chi^{(i)} \hat{\nabla} \chi^{(i)} \cdot \boldsymbol{n} d\hat{S} - \int_{\partial\hat{\Omega}_{per}} \chi^{(i)} \hat{\nabla} \chi^{(i)} \cdot \boldsymbol{n} d\hat{S}.$$

The first term on the right-hand side of this equations vanishes by periodicity. Applying the boundary condition on $\partial\hat{\Omega}_{per}$ contained in (96) leads to

$$-\int_{\partial\hat{\Omega}_{per}} \chi^{(i)} \boldsymbol{e}_i \cdot \boldsymbol{n} d\hat{S} = \int_{\hat{V}_{per}} |\hat{\nabla} \chi^{(i)}|^2 d\hat{V} > 0.$$